PERGAMON

International Journal of Multiphase Flow 28 (2002) 21–50

International Journal of Multiphase Flow

www.elsevier.com/locate/ijmulflow

The role of thermal disequilibrium in critical two-phase flow

E. Valero *, I.E. Parra

E.T.S.I. Aeronáuticos, Universidad Politécnica de Madrid, Pza. Cardenal Cisneros, 3, 28040 Madrid, Spain

Received 30 April 2001; received in revised form 30 August 2001

Abstract

An asymptotic analysis of a mechanistic Equal Velocity Unequal Temperature (EVUT) model has been developed to predict critical flashing flows. The obtained results have been compared with those coming from the Homogeneous Equilibrium Model (HEM) and some experimental data extracted from Marviken test series. In spite of its simplicity, the developed non-equilibrium model not only gives a good approach to experimental measures but also explains the complex behavior shown by critical blowdowns of pressurized vessels. © 2001 Elsevier Science Ltd. All rights reserved.

Keywords: Critical flow; Flashing; Critical blowdown; Two-phase flow

1. Introduction

Determination of mass flow rates in critical flows of vapor–liquid mixtures is a problem of great importance in many engineering processes (analysis and design of nuclear power plants, handling of liquefied gases, analysis of cooling systems, etc.). Many significant aspects can influence critical two-phase flows: geometry, flow regime, fluid history, thermal disequilibrium, etc., and, despite the large amount of work done in the past, the problem remains open. A lot of empirical and analytical correlations have been developed to determine critical velocities in particular cases (see, f.i., the reviews of Saha, 1978; Wallis, 1980; Elias and Lellouche, 1994), but all of them fail to give either accurate results or physical justification in general situations.

An interesting and very common example of critical two-phase flow arises when a pressurized vessel containing subcooled liquid at high temperature is suddenly opened (through a nozzle, a pipe or a crack) to the ambient conditions. After a few milliseconds, the liquid discharges quasi-steadily through the exit channel, where flashing arises, presenting a critical behavior. The

* Corresponding author.
E-mail addresses: valero@dmae.upm.es (E. Valero), parra@dmae.upm.es (I.E. Parra).

PII: S0301-9322(01)00064-7

mentioned review papers and some specific works on flashing flows (Ardron, 1978; Dobran, 1987; Sami and Doung, 1989; Bilicki and Kestin, 1990; Deligiannis and Cleaver, 1990; Elias and Chambré, 1984, 1993) point out the importance of considering thermal disequilibrium and slip between phases to predict critical mass flow rates in this particular case.

When void fractions are small, interphase slip can be neglected. In such a case, the fluid can be considered as a bubbly mixture where the vapor bubbles are dragged along by the liquid. Moreover, the thermal disequilibrium between phases only becomes significant when the bubble nucleation is incipient and, as a result, the void fraction is very small. In fact, the Homogeneous Equilibrium Model (HEM – no slip, no thermal disequilibrium) is a good approximation in many practical situations. Only discharges through very short nozzles and those presenting high inlet subcoolings are not well modeled by such an approximate model.

In the present work, the significance of thermal disequilibrium is analyzed in dispersed bubbly flows under critical conditions. To do that, a mechanistic Equal Velocity Unequal Temperature (EVUT) model is chosen. When the liquid pressure is below the corresponding saturation pressure, the fluid is modeled as an homogeneous mixture of metastable liquid and spherical bubbles of saturated vapor. The metastability degree of the mixture, which is sized by the amount that pressure is below the saturation value, determines the rate of bubble nucleation. As slip between phases is not considered, the scope of this study is restricted to the range of small void fractions, $\alpha < 0.3$. Consequently, from a practical point of view, this analysis will be mainly applicable to flashing flows in short non-divergent ducts.

Results corresponding to critical blowdowns of pressurized vessels are compared with HEM predictions and some available experimental data. For subcooled blowdowns, the predicted mass flow rates, which are greater than those given by the equilibrium model, fit well with experimental results. However, for saturated blowdowns, the presence of bubble nuclei entering the exit duct must be considered in order that EVUT model gives accurate predictions.

The paper is organized as follows. Section 2 states the basic equations which describe the flow through a discharging nozzle. In Section 3, the results given by the HEM approach are reviewed as a simplification of the EVUT model. Section 4 summarizes the main results arising from the asymptotic analysis of the non-equilibrium model. Comparison between analytical results and available experimental data is shown in Section 5. Finally, the principal concluding remarks are summarized in Section 6.

2. Basic equations (EVUT model)

Basically, the EVUT model analyzed here consists of the three mixture conservation equations (mass, momentum and energy), a vapor generation law and the corresponding state equations. The main assumptions used in the model are: the flow is one-dimensional, steady and adiabatic, friction losses and gravitational effects are neglected and the fluid is either a subcooled liquid or an homogeneous mixture of metastable liquid and spherical bubbles of saturated vapor.

Using these assumptions, the conservation laws can be stated as (see, f.i., Bouré, 1978)

$$\bar{\rho}\bar{v}\bar{A} = \bar{\phi}, \tag{1}$$

$$\bar{\rho}\bar{v}\frac{\mathrm{d}\bar{v}}{\mathrm{d}z}+\frac{\mathrm{d}\bar{P}}{\mathrm{d}z}=0, \tag{2}$$

$$\bar{h}+\frac{\bar{v}^2}{2}=\bar{h}_{\mathrm{d}}. \tag{3}$$

Quantities $\bar{\rho}, \bar{v}, \bar{P}$ and $\bar{h}$ are, respectively, density, axial velocity, pressure and specific enthalpy of the mixture. The constant $\bar{\phi}$ is the mass flow rate through the nozzle. At each section, $\bar{A}$ is the cross-sectional area, which is assumed to be a non-increasing function of z (the distance from the nozzle inlet) in the remainder of this paper. Subscript "d" denotes magnitudes corresponding to the inlet section.

To deduce (3), stagnation conditions and zero velocity have been considered at the inlet. Such an assumption is physically consistent with many practical situations, where pressurized tanks or vessels are discharged to ambient conditions through small nozzles or cracks.

The following approximate expressions will be considered for density and specific enthalpy of each phase:

$$\bar{\rho}_{\mathrm{L}}=\bar{\rho}_{\ell}(1+k_{\mathrm{s}}(\bar{P}-\bar{P}_{\mathrm{sd}})-k_{\beta}(\bar{T}-\bar{T}_{\mathrm{d}})),\quad \bar{\rho}_{\mathrm{G}}=\frac{\bar{P}}{R_{\mathrm{w}}\bar{T}_{\mathrm{s}}(\bar{P})}, \tag{4}$$

$$\bar{h}_{\mathrm{L}}=\bar{h}_{\mathrm{Ld}}+C_{\ell}(\bar{T}-\bar{T}_{\mathrm{d}})+\frac{\bar{P}-\bar{P}_{\mathrm{sd}}}{\bar{\rho}_{\ell}},\quad \bar{h}_{\mathrm{G}}=\bar{h}_{\mathrm{Ld}}+L+C_{\mathrm{pv}}(\bar{T}_{\mathrm{s}}(\bar{P})-\bar{T}_{\mathrm{d}}). \tag{5}$$

The use of the above relationships is justified by many critical blowdown experiments, where the exit pressure is by about 20% under the inlet saturation pressure. Such a percentage corresponds to saturation temperature variations 5% below the inlet temperature. The parameters appearing in these expressions are the following thermodynamic magnitudes (calculated at temperature $\bar{T}_{\mathrm{d}}$ under saturated conditions): $\bar{\rho}_{\ell}$, liquid density; k_{s}, isothermal liquid compressibility; k_{β}, volumetric expansion coefficient of the liquid; $\bar{P}_{\mathrm{sd}}$, saturated pressure; $\bar{h}_{\mathrm{Ld}}$, liquid specific enthalpy; C_{ℓ} and C_{pv}, liquid and gas constant pressure specific heat capacities; L, latent heat of vaporization. Furthermore, the variable $\bar{T}$ is the liquid temperature and the function $\bar{T}_{\mathrm{s}}(\bar{P})$ is the saturation temperature at pressure $\bar{P}$. For small temperature oscillations, such a function and its inverse, $\bar{P}_{\mathrm{s}}(\bar{T})$, can be approximated making use of the Clausius–Clapeyron approximation near the saturation point corresponding to the inlet temperature

$$\frac{\mathrm{d}\bar{T}_{\mathrm{s}}}{\mathrm{d}\bar{P}}=\frac{\bar{T}_{\mathrm{s}}}{L\bar{\rho}_{\mathrm{G}}},\quad \bar{T}_{\mathrm{s}}(\bar{P}_{\mathrm{sd}})=\bar{T}_{\mathrm{d}}. \tag{6}$$

Except for the second relation of (4), the approximations used in state equations (4) and (5) are linearizations around the saturation point $(\bar{T}_{\mathrm{d}}, \bar{P}_{\mathrm{sd}})$. In fact, as saturation temperature varies slightly along the channel, vapor density also behaves almost linearly with pressure. Furthermore, when temperatures are high and the use of the ideal gas law introduces significant errors, the results are improved to a great extent after using the isothermal law

$$\frac{\bar{P}}{\bar{\rho}_{\mathrm{G}}}=\frac{\bar{P}_{\mathrm{sd}}}{\bar{\rho}_{\mathrm{g}}} \tag{7}$$

instead of the second expression of (4) ($\bar{\rho}_g$ is the saturated vapor density at $\bar{T}_d$). For instance, for the inlet conditions present in Marviken tests (analyzed in Section 5), the above expression predicts saturated vapor densities with relative errors of 2% for temperatures 30 °C below the inlet temperature.

To close the system (1)–(3) a constitutive law of vapor generation, relating the rate of interfacial mass transfer with other variables involved in the problem, is needed. To obtain it, both a rate of bubble generation and a bubble growth law will be considered. Nucleation Theory (Blander and Katz, 1975; Deligiannis and Cleaver, 1990) provides the rate of bubble production

$$J = NB \exp\left(-\frac{16\pi\sigma^3\psi}{3k_B\bar{T}\overline{\Delta P}^2}\right), \tag{8}$$

where N is the number of molecules per unit volume in the liquid phase, k_B is the Boltzmann constant, σ is the surface tension at the gas–liquid interface and the parameter $B = \sqrt{2\sigma/\pi m}$ is the kinetic factor (m is the molecular weight). The magnitude $\overline{\Delta P} = \bar{P}_s(\bar{T}) - \bar{P}$, termed the pressure undershoot, sizes the supersaturation degree of the liquid phase. Alternatively, if such a quantity is negative, it measures the liquid phase subcooling. Expression (8) is valid for positive values of $\overline{\Delta P}$, otherwise the nuclei production is null.

The exponential factor ψ is introduced to take into account heterogeneous nucleation phenomena (wall cavities, liquid impurities, bubble clustering, etc.). Empirical correlations relating ψ with other relevant depressurization parameters (as liquid temperature and rate of depressurization) are proposed by some authors, see, f.i., Deligiannis and Cleaver (1992, 1993), Alamgir and Lienhard (1981), Elias and Chambré (1993) and Barták (1990). However, in this work, the inhomogeneity factor ψ will be considered as an empirically adjusted constant parameter. This assumption limits the scope of the obtained results to these cases where fluid conditions and flow characteristics are similar to those present in the data used to adjust ψ.

On the other hand, the bubble growth is assumed to be thermally controlled, i.e., the interfacial heat transfer is totally spent on the production of the new phase (see, f.i., Nigmatulin, 1991, Vol. 1, Section 2.9)

$$\frac{d}{dt}\left(\frac{4\pi}{3}\bar{r}^3\bar{\rho}_G\right) = Nu 2\pi\bar{r}\frac{k_\ell\overline{\Delta T}}{L}. \tag{9}$$

Quantities $\bar{r}$ and $\overline{\Delta T} = \bar{T} - \bar{T}_s(\bar{P})$ are, respectively, the bubble radius and the liquid supersaturation degree. Last magnitude is related to the mixture pressure undershoot through $\bar{T} = \bar{T}_s(\bar{P} + \overline{\Delta P})$. Other parameters are: k_ℓ, the liquid thermal conductivity and Nu, a Nusselt number based in the bubble diameter which accounts for the size of the interfacial thermal boundary layer. The use of the above expression implies that the influence of bubble growth becomes significant when bubbles have left behind their initial growth stages controlled by surface tension and inertia forces.

A suitable expression for Nu, valid in a wide range of moderate and weak superheats, is given by

$$Nu = 2 + (2Ja)^{1/3} + \frac{12Ja}{\pi},$$

where $Ja = (C_\ell \bar{\rho}_\ell \overline{\Delta T})/(\bar{\rho}_g L)$ is the Jacobs number. However, moderate and high mixture superheats are expected to arise only in thin layers after the nucleation points. Thus, in order not to complicate calculations unnecessarily, the Nusselt number $Nu = 2$, corresponding to weak superheats ($Ja \ll 1$), will be used in the following.

After using expressions (8) and (9), the following void fraction evolution law is obtained (see Appendix A):

$$\alpha(z) = \frac{4\pi NB(2k_\ell)^{3/2}}{3L^{3/2}} \int_{z_n}^{z} \left(\int_{z_0}^{z} \frac{\overline{\Delta T}(\bar{z}_0)\, \mathrm{d}\bar{z}_0}{\bar{\rho}_G(\bar{z}_0)^{1/3} \bar{v}(\bar{z}_0)} \right)^{3/2} \frac{(1-\alpha(z_0))\bar{A}(z_0)\bar{F}(\overline{\Delta P}(z_0))}{\bar{A}(z)\bar{v}(z)\bar{\rho}_G(z)}\, \mathrm{d}z_0, \tag{10}$$

where the function $\bar{F}(\overline{\Delta P})$ is defined as

$$\bar{F}(\overline{\Delta P}) = \begin{cases} \exp\left(-\frac{16\pi\sigma^3\psi}{3k_B\bar{T}\overline{\Delta P}^2}\right), & \overline{\Delta P} > 0, \\ 0, & \overline{\Delta P} \leqslant 0. \end{cases}$$

The symbol z_n terms the nearest position to the pipe inlet where the pressure undershoot, $\overline{\Delta P}$, becomes positive. Upstream from z_n, the void fraction is null and the fluid is a subcooled liquid. In particular, $z_n = 0$ for $\overline{\Delta P}_d = 0$.

3. The Homogeneous Equilibrium Model (HEM)

When the constitutive relation (10) is substituted by the equilibrium condition

$$\bar{T} = \bar{T}_s(\bar{P}) \quad \text{or} \quad \overline{\Delta P} = 0,$$

the HEM results (the fluid is either a subcooled liquid, $\alpha = 0$ and $\overline{\Delta P} < 0$, or an equilibrium two-phase mixture, $\alpha > 0$ and $\overline{\Delta P} = 0$). In this model, density can be expressed as a function of pressure and specific enthalpy. For equilibrium mixtures, the function takes the form

$$\bar{\rho} = \bar{\rho}_m(\bar{P}, \bar{h}) = \frac{\bar{\rho}_G \bar{\rho}_L (\bar{h}_G - \bar{h}_L)}{\bar{\rho}_G \bar{h}_G - \bar{\rho}_L \bar{h}_L + (\bar{\rho}_L - \bar{\rho}_G)\bar{h}}.$$

When the fluid is a subcooled liquid, last equation must be replaced by the subcooled relation $\bar{\rho} = \bar{\rho}_L(\bar{P}, \bar{h})$ obtained after eliminating $\bar{T}$ between the leading expressions of (4) and (5). Using such a function and Eq. (1) a differential equation describing the pressure evolution along the nozzle is obtained

$$\left(1 - \frac{\bar{\phi}^2}{(\bar{\rho}\bar{v}_c\bar{A})^2}\right) \frac{\mathrm{d}\bar{P}}{\mathrm{d}z} = \frac{\bar{\phi}^2 \bar{A}'}{\bar{\rho}\bar{A}^3}, \quad \text{where } \frac{1}{\bar{v}_c^2} = \left(\frac{\partial\bar{\rho}}{\partial\bar{P}}\right)_{\bar{h}} + \frac{1}{\bar{\rho}}\left(\frac{\partial\bar{\rho}}{\partial\bar{h}}\right)_{\bar{P}}. \tag{11}$$

Enthalpy and pressure are related through the algebraic expressions (1) and (3). The positive quantity $\bar{v}_c$ is the local sound speed, which is a discontinuous function along the liquid saturation boundary, $\bar{h} = \bar{h}_L(\bar{P}, \bar{T}_s(\bar{P}))$. In particular, for temperatures less enough than the critical temperature the sound speed falls from the value obtained for monophasic liquids ($\bar{v}_c^2 \simeq 1/\bar{\rho}_\ell k_s$) to the low value corresponding to incipient saturated mixtures:

$$\bar{v}_{cd} \simeq \frac{\bar{P}_{sd} L}{\bar{\rho}_\ell R_w \bar{T}_d \sqrt{C_\ell \bar{T}_d}}. \tag{12}$$

To obtain last approximate expression, vapor–liquid density ratio and liquid compressibility have been neglected.

The classical HEM critical condition results when the leading coefficient of Eq. (11) is cancelled out

$$\bar{v} = \frac{\bar{\phi}}{\bar{A}\bar{\rho}} = \bar{v}_c(\bar{P}, \bar{h}). \tag{13}$$

At those points where last condition is fulfilled, the pressure profiles given by Eq. (11) present a turning point with vertical tangent (see Fig. 1(b)). However, such pressure profiles also present an abrupt change of tangent when saturation pressure is reached. Therefore, when the solutions of (11) attain the saturation boundary with velocities greater than the sound velocity for saturated mixtures ($\bar{\phi}/\bar{A}\bar{\rho} > \bar{v}_{cd}$), the z derivative of $\bar{P}$ changes of sign and pressure profiles present discontinuous turning points at the saturation pressure (see Fig. 1(a)). In such a case, the critical condition takes the form (see Collins, 1978)

$$\bar{P} = \bar{P}_{sd}, \tag{14}$$

which arises when the fluid velocity at the critical point is greater than the mixture sound speed at the saturation limit, $\bar{v}_{cd}$. Owing to the small values of the liquid compressibility ($\bar{\rho} \simeq \bar{\rho}_\ell$),

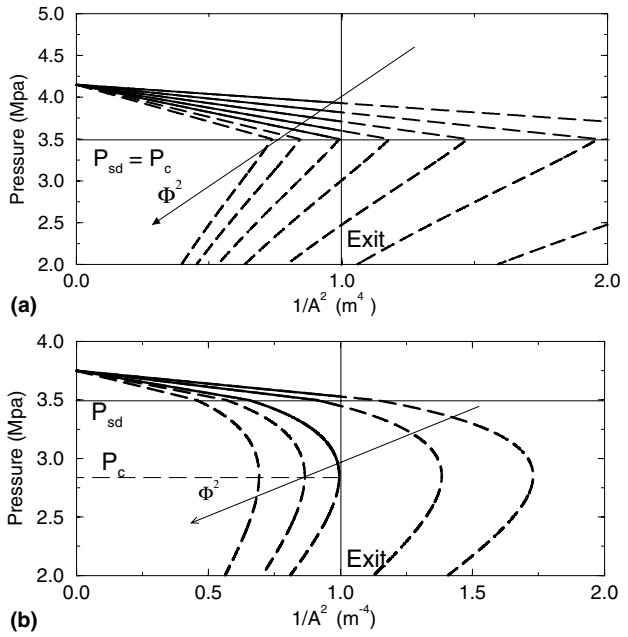

Fig. 1. HEM pressure profiles along a nozzle with exit area $\bar{A}_a = 1\ m^2$ for (a) $-2\overline{\Delta P}_d > \bar{\rho}_\ell \bar{v}_{cd}^2$ and (b) $-2\overline{\Delta P}_d < \bar{\rho}_\ell \bar{v}_{cd}^2$ (solid lines represent physically admissible solutions).

Eq. (2) can be easily integrated and the applicability range of condition (14) can be analytically stated as

$$-2\overline{\Delta P}_{\mathrm{d}} - \bar{\rho}_{\ell}\bar{v}_{\mathrm{cd}}^2 \geqslant 0. \tag{15}$$

If the above quantity is negative, the applicable critical condition is (13).

4. Asymptotic analysis of the EVUT model

To analyze the non-equilibrium model proposed in Section 2, the following non-dimensional variables are chosen:

$$\rho = \bar{\rho}/\bar{\rho}_{\ell}, \quad v = \bar{v}/\bar{v}_{\mathrm{cd}}, \quad h = (\bar{h} - \bar{h}_{\mathrm{Ld}})/\bar{v}_{\mathrm{cd}}^2, \quad A = \bar{A}/\bar{A}_{\mathrm{a}}, \quad y = z/z_{\mathrm{a}},$$

$$P = \frac{\bar{P} - \bar{P}_{\mathrm{sd}}}{\bar{\rho}_{\ell}\bar{v}_{\mathrm{cd}}^2}, \quad \Delta P = \frac{\overline{\Delta P}}{\bar{\rho}_{\ell}\bar{v}_{\mathrm{cd}}^2}, \quad T = \frac{(\bar{T} - \bar{T}_{\mathrm{d}})R_{\mathrm{w}}}{\bar{v}_{\mathrm{cd}}^2}, \quad \Delta T = \frac{\overline{\Delta T}R_{\mathrm{w}}}{\bar{v}_{\mathrm{cd}}^2}.$$

Subscript "a" refers to exit section, thus z_{a} and $\bar{A}_{\mathrm{a}}$ are, respectively, the nozzle length and the nozzle exit cross-sectional area.

The non-dimensional system resulting from Eqs. (1)–(6) and (10) is

$$\rho v A = \phi, \tag{16}$$

$$\rho v \frac{\mathrm{d}v}{\mathrm{d}y} + \frac{\mathrm{d}P}{\mathrm{d}y} = 0, \tag{17}$$

$$h + \frac{v^2}{2} = -\Delta P_{\mathrm{d}}, \tag{18}$$

$$\rho = (1-\alpha)(1 + c^2 P - c_{\beta}^2 T) + \varepsilon\alpha\frac{\theta_{\mathrm{d}} + P}{\theta_{\mathrm{d}} + \varepsilon T_{\mathrm{s}}(P)}, \tag{19}$$

$$\rho h = (1-\alpha)(1 + c^2 P - c_{\beta}^2 T)(\mu_{\ell} T + P) + \alpha\frac{\varepsilon(\theta_{\mathrm{d}} + P)(l + \mu_v T_{\mathrm{s}}(P))}{\theta_{\mathrm{d}} + \varepsilon T_{\mathrm{s}}(P)}, \tag{20}$$

$$\frac{\mathrm{d}T_{\mathrm{s}}}{\mathrm{d}P} = \frac{(\theta_{\mathrm{d}} + \varepsilon T_{\mathrm{s}})^2}{\varepsilon^2 l(\theta_{\mathrm{d}} + P)}, \quad T_{\mathrm{s}}(0) = 0, \tag{21}$$

$$\alpha(y) = C\int_{y_n}^{y}\left(\int_{y_0}^{y}\frac{\Delta T(\bar{y}_0)\,\mathrm{d}\bar{y}_0}{v(\bar{y}_0)\rho_{\mathrm{G}}(\bar{y}_0)^{1/3}}\right)^{3/2}\frac{(1-\alpha(y_0))A(y_0)F(\Delta P(y_0))}{A(y)v(y)\rho_{\mathrm{G}}(y)}\,\mathrm{d}y_0, \tag{22}$$

where

$$F(\Delta P) = \begin{cases} \exp\left(-\frac{a}{\Delta P^2}\right), & \Delta P > 0, \\ 0, & \Delta P \leqslant 0, \end{cases} \quad \text{and} \quad \rho_{\mathrm{G}} = \varepsilon\frac{\theta_{\mathrm{d}} + P}{\theta_{\mathrm{d}} + \varepsilon T_{\mathrm{s}}(P)}.$$

The non-dimensional parameters appearing in the previous set of equations are

$$\phi = \frac{\bar{\phi}}{\bar{\rho}_\ell \bar{v}_{cd} \bar{A}_a}, \quad \Delta P_d = \frac{(\bar{P}_{sd} - \bar{P}_d)}{\bar{\rho}_\ell \bar{v}_{cd}^2}, \quad c^2 = k_s \bar{\rho}_\ell \bar{v}_{cd}^2, \quad c_\beta^2 = k_\beta \bar{v}_{cd}^2 / R_w, \quad \varepsilon = \frac{\bar{P}_{sd}}{\bar{\rho}_\ell R_w \bar{T}_d},$$

$$\theta_d = \frac{\bar{P}_{sd}}{\bar{\rho}_\ell \bar{v}_{cd}^2}, \quad \mu_\ell = \frac{C_\ell}{R_w}, \quad \mu_v = \frac{C_{pv}}{R_w}, \quad l = \frac{L}{\bar{v}_{cd}^2}, \quad C = \frac{4\pi NB}{3} \left(\frac{2k_\ell}{l R_w \bar{\rho}_\ell} \right)^{3/2} \left(\frac{z_a}{\bar{v}_{cd}} \right)^{5/2},$$

$$a = \frac{16\pi\sigma^3 \psi}{3k_B \bar{T}_d \bar{\rho}_\ell^2 \bar{v}_{cd}^4}.$$

The system (16)–(22) must be completed with the boundary conditions

$$P(0) = -\Delta P_d, \quad P(1) = P_a, \tag{23}$$

which serve, respectively: as initial condition in the integration of the differential equation (17) and as physical condition in the determination of the mass flow rate ϕ.

To deduce Eq. (18), it has been considered that pure liquid enters the nozzle ($\alpha_d = 0$). The quantity $-\Delta P_d$, which is usually non-negative, is the liquid subcooling degree at the nozzle inlet. Sometimes, during the rapid depressurization of a vessel, the vessel liquid may reach superheated states ($\Delta P_d > 0$). However, in such a case ΔP_d used to be negligible compared with the undershoots arising inside of the pipe, because of the relatively slow vessel depressurization rates.

Using Eqs. (16) and (18)–(21) and having into account that $T = T_s(P + \Delta P)$, the magnitudes ρ, v and P can be obtained as functions of α and ΔP. Thus a differential relation between α and ΔP comes from Eq. (17). Integrating such a relation together with the vapor generation law (29) and boundary conditions (23) solves the problem.

An approximate model of the problem (16)–(23) will be developed in the sequel. Such an asymptotic model corresponds to the limit $l^{-1} \ll \varepsilon \ll 1$, which is valid when inlet temperatures are under the 90% of the substance critical temperature. Furthermore, the smallness of the non-dimensional liquid coefficients of isothermal compressibility and volumetric expansion, c^2 and c_β^2, and the exponentially large value of the bubble production coefficient, C, will be also taken into account. Under these assumptions, the following approximate equations come from the system (16)–(23):

$$\rho = \frac{1}{1+w}, \quad v = \frac{\phi(1+w)}{A}, \tag{24}$$

$$T_s(P) = \frac{\theta_d^2}{\varepsilon^2 l} \log\left(1 + \frac{P}{\theta_d}\right), \tag{25}$$

$$\theta_d \log\left(1 + \frac{P + \Delta P}{\theta_d}\right) + w\left(1 + \frac{P}{\theta_d}\right) = 0, \tag{26}$$

$$\frac{\phi^2}{A^2} \frac{dw}{dy} + \frac{dP}{dy} = \frac{\phi^2 (1+w) A'}{A^3}, \tag{27}$$

$$w(y)\left(1+\frac{P(y)}{\theta_{\mathrm{d}}}\right)=\frac{C\theta_{\mathrm{d}}^{3}}{\phi^{5/2}\varepsilon^{9/2}l^{3/2}}\int_{y_n}^{y}\left(\int_{y_0}^{y}\frac{A(\bar{y}_0)\log\left(1+(\Delta P(\bar{y}_0)/(\theta_{\mathrm{d}}+P(\bar{y}_0)))\right)\mathrm{d}\bar{y}_0}{\left(1+(P(\bar{y}_0)/\theta_{\mathrm{d}})\right)^{1/3}(1+w(\bar{y}_0))}\right)^{3/2}\times\frac{A(y_0)}{1+w(y_0)}F(\Delta P(y_0))\,\mathrm{d}y_0 \tag{28}$$

$$P(0)=-\Delta P_{\mathrm{d}}, \tag{29}$$

$$P(1)=P_{\mathrm{a}}. \tag{30}$$

In the above system, the volumetric ratio, $w=\alpha/(1-\alpha)$, is introduced in place of the void fraction, α. Both magnitudes, volumetric ratio and void fraction, must be taken identically zero until the pressure undershoot becomes positive at position y_n, because the integrand in the second member of Eq. (28) is null for non-positive values of ΔP.

Moreover, to obtain Eq. (26), the identity $\varepsilon^3 l^2=\mu_\ell\theta_{\mathrm{d}}$ has been taken into account. Such an equality follows from the use of the approximate expression (12) of the characteristic velocity, $\bar{v}_{\mathrm{cd}}$, which was obtained neglecting terms up to order ε, c^2 and c_β^2.

When the ideal gas law in (4) is substituted by the linear approximation (7), the same asymptotic model (Eqs. (24)–(30)) follows. However, the significant parameters of the problem must be calculated making use of the quantity $\bar{P}_{\mathrm{sd}}/\bar{\rho}_{\mathrm{g}}\bar{T}_{\mathrm{d}}$ instead of the gas constant R_{w}. For instance, the vapor–liquid density ratio, the coefficient C and the characteristic mixture sound speed now read, respectively,

$$\varepsilon=\frac{\bar{\rho}_{\mathrm{g}}}{\bar{\rho}_\ell},\quad C=\frac{4\pi NB}{3}\left(\frac{2k_\ell\bar{\rho}_{\mathrm{g}}\bar{T}_{\mathrm{d}}}{l\bar{P}_{\mathrm{sd}}\bar{\rho}_\ell}\right)^{3/2}\left(\frac{z_{\mathrm{a}}}{\bar{v}_{\mathrm{cd}}}\right)^{5/2},\quad \bar{v}_{\mathrm{cd}}=\frac{\bar{\rho}_{\mathrm{g}}L}{\bar{\rho}_\ell\sqrt{C_\ell\bar{T}_{\mathrm{d}}}}. \tag{31}$$

The differential equation

$$\frac{\mathrm{d}\Delta P}{\mathrm{d}y}=\left(\frac{\phi^2}{A^2}-\left(1+\frac{P}{\theta_{\mathrm{d}}}-\frac{\phi^2 w}{A^2\theta_{\mathrm{d}}}\right)\left(1+\frac{P+\Delta P}{\theta_{\mathrm{d}}}\right)\right)\frac{\mathrm{d}w}{\mathrm{d}y}-\frac{\phi^2A'}{A^3}\left(1+\left(1+\frac{P+\Delta P}{\theta_{\mathrm{d}}}\right)\frac{w}{\theta_{\mathrm{d}}}\right)(1+w), \tag{32}$$

which describes the pressure undershoot evolution, follows from relations (26) and (27). The integrodifferential system (28) and (32), Eq. (26) and the boundary condition (29) constitute an initial-value problem, which can be solved for each fixed value of the non-dimensional mass flux, ϕ.

The mass flux corresponding to a particular discharge problem will be determined using the exit boundary condition (30). Here, in contrast to the HEM model, where critical phenomena can arise, such an exit condition is always applicable. However, as it will be seen later, if P_{a} is below a critical bound, P_{c}, the pressure profile evolves steeply under P_{c} in a thin layer near the exit and the corresponding mass flux coincides practically with that obtained for $P_{\mathrm{a}}=P_{\mathrm{c}}$. Therefore, from a practical point of view, though analytically condition (30) ever applies, such a condition determines the discharge mass flux only when P_{a} ranges between P_{c} and $-\Delta P_{\mathrm{d}}$. For exit pressures below

the critical value, as it similarly happens in the HEM model, the mass flux apparently does not depend on the exit pressure.

To see that, the integrodifferential system (28) and (32) is analyzed in the following paragraphs.

In all sections upstream from $A_n = A(y_n)$, the pressure undershoot is negative and the volumetric ratio is null. Thus, Eq. (32) reduces to

$$\frac{\mathrm{d}\Delta P}{\mathrm{d}y} = -\frac{\phi^2 A'}{A^3} \quad \text{for } y \leqslant y_n, \tag{33}$$

which implies ($\Delta P(0) = \Delta P_\mathrm{d}$)

$$\Delta P = \Delta P_\mathrm{d} + \frac{\phi^2}{2A^2} \quad \text{for } y \leqslant y_n. \tag{34}$$

Therefore, provided that inlet stagnation conditions are subcooled ($\Delta P_\mathrm{d} < 0$), the point y_n (where pressure undershoot becomes null) is determined by the condition

$$\Delta P_\mathrm{d} + \frac{\phi^2}{2A_n^2} = 0. \tag{35}$$

For $\phi^2 < -2\Delta P_\mathrm{d}$ Eq. (35) has no solutions inside of a convergent nozzle, because A is greater than unity at all sections. Consequently, everywhere in the nozzle the conditions are subcooled and the volumetric ratio is null. Thus, as Eq. (26) implies

$$P = -\Delta P \tag{36}$$

for $w = 0$, non-dimensional mass fluxes less than $-2\Delta P_\mathrm{d}$ correspond to exit pressures greater than the inlet saturated pressure ($P_\mathrm{a} > 0$).

On the other hand, if $\phi^2 \geqslant -2\Delta P_\mathrm{d}$, there exists inside of the nozzle a section fulfilling Eq. (35) ($A_n \geqslant 1$, $0 \leqslant y_n \leqslant 1$). The case of $y_n = 0$ corresponds to inlet saturated conditions ($\Delta P_\mathrm{d} = 0$).

To understand the phenomena arising downstream from the saturation point y_n, the exponential character of the volumetric ratio evolution law (28) must be considered. Thus, although the integrand of such an integral expression is non-null for positive pressure undershoots, it remains exponentially small along a metastable region behind y_n. In such a region, not only the volumetric ratio can be neglected but subcooled expressions (34) and (36) can be also applied. However, the situation evolves steeply at point y_m (the so-called point of flashing), defined as the position where the volumetric ratio derivative ($\mathrm{d}w/\mathrm{d}y$) becomes as important as the other terms in Eq. (32). Just after section $A_m = A(y_m)$, significant changes arise inside a thin nucleation layer.

To analyze the fluid evolution in such a nucleation layer, new stretched variables

$$b = \frac{\Delta P - \Delta P_m}{\beta}, \quad s = \frac{y - y_m}{\eta}$$

are introduced in Eqs. (32) and (28)

$$\frac{\beta}{\eta}\frac{\mathrm{d}b}{\mathrm{d}s} = \frac{(\phi^2/A_{\mathrm{m}}^2) + (\Delta P_m/\theta_{\mathrm{d}}) - 1}{\eta}\frac{\mathrm{d}w}{\mathrm{d}s} - \frac{\phi^2 A'_m}{A_m^3},$$
$$w = \left(\frac{\eta A_{\mathrm{m}}}{\phi}\right)^{5/2}\left(\frac{-\theta_{\mathrm{d}}^2\log(1-(\Delta P_{\mathrm{m}}/\theta_{\mathrm{d}}))}{\varepsilon^3 l(1-(\Delta P_m/\theta_{\mathrm{d}}))}\right)^{3/2} C\mathrm{e}^{-a/\Delta P_m^2}\int_{-\infty}^{s}(s-x)^{3/2}\mathrm{e}^{(2a\beta/\Delta P_m^3)b(x)}\,\mathrm{d}x. \tag{37}$$

The above approximate expressions have been obtained assuming that the nucleation layer characteristic magnitudes are small enough, $\eta \ll 1$ and $w \sim \beta \ll \Delta P_{\mathrm{m}} = \Delta P(y_m)$. Such an assumption will be verified later.

At the point of flashing y_m, according to its definition, the orders of all terms in Eq. (37) must be equal. Thus, the identities

$$\frac{\beta}{\eta} = \left|\frac{\phi^2}{A_m^2} + \frac{\Delta P_{\mathrm{m}}}{\theta_{\mathrm{d}}} - 1\right|\left(\frac{A_{\mathrm{m}}}{\phi}\right)^{5/2}\left(\frac{-\theta_{\mathrm{d}}^2\log(1-(\Delta P_{\mathrm{m}}/\theta_{\mathrm{d}}))}{\varepsilon^3 l(1-(\Delta P_m/\theta_{\mathrm{d}}))}\right)^{3/2} C\mathrm{e}^{-a/\Delta P_m^2}\eta^{3/2} = \frac{\phi^2|A'_m|}{A_m^3} \tag{38}$$

are fulfilled by suitable values of η, β and ΔP_m. With the above assumptions Eq. (37) will read

$$\frac{\mathrm{d}b}{\mathrm{d}s} = 1 \pm \frac{\mathrm{d}}{\mathrm{d}s}\int_{-\infty}^{s}(s-x)^{3/2}\mathrm{e}^{(2a\beta/\Delta P_m^3)b(x)}\,\mathrm{d}x.$$

Then, in order that volumetric ratio and pressure undershoot present fluctuations of the same order, the parameter β should be chosen to allow variations of order unity in the integral member of last equation. An adequate value to cover this requirement is

$$\beta = \frac{\Delta P_m^3}{2a}. \tag{39}$$

In relations (38) and (39), the representative values of pressure undershoot and cross-sectional area $(\Delta P_m, A_m)$ are taken at section y_m, where, in a first approximation, subcooled expressions (34) and (36) are still valid. Then, these magnitudes fulfill the following relation:

$$\Delta P_m = \Delta P_{\mathrm{d}} + \frac{\phi^2}{2A_m^2} = -P(y_m). \tag{40}$$

Eqs. (38)–(40) constitute a four-order non-linear system of equations, whose solutions η, β, y_m and ΔP_m define adequate stretched variables, b and s, to study the flow inside the nucleation layer. Eliminating $\eta, \beta, \phi/A_m$ from Eqs. (38)–(40), the non-linear relation

$$\frac{|(2+(1/\theta_{\mathrm{d}}))\Delta P_m - 2\Delta P_{\mathrm{d}} - 1|}{(2\Delta P_m - 2\Delta P_{\mathrm{d}})^{15/4}}\left|\frac{A_m}{A'_{\mathrm{m}}}\right|^{5/2}\left(\frac{-\Delta P_m^3\theta_{\mathrm{d}}^2\log(1-(\Delta P_m/\theta_{\mathrm{d}}))}{2a\varepsilon^3 l(1-(\Delta P_m/\theta_{\mathrm{d}}))}\right)^{3/2} C\mathrm{e}^{-a/\Delta P_m^2} = 1 \tag{41}$$

results. Last equation relates the unknown quantity ΔP_m to characteristic parameters of the discharge problem. All these parameters are known but the ratio between the cross-sectional area and its derivative at point y_m. Such a position depends on the a priori unknown parameter ϕ (see Eq. (40)). However, owing to the exponential character of relation (41), the values of ΔP_m fulfilling such a relation mainly depend on the non-dimensional parameter a and hardly vary with other involved data. In fact, it can be easily proven that variations of order unity in A_m/A'_m imply errors of order β in the evaluation of ΔP_m. Then, to simplify the calculations, the solution of (41)

corresponding to representative values of ϕ and A_m/A'_m can be used in practice. When a more exact value of ϕ is known, further adjustment of ΔP_m is unnecessary.

Eq. (41) is solvable in the region: $0 \leqslant \Delta P_{\mathrm{m}} \leqslant \theta_{\mathrm{d}}$ for any fixed value of A_m/A'_m. The minimal solution of Eq. (41) (for which the symbol ΔP_m will be reserved in the sequel) corresponds to the minimum pressure undershoot which makes the nucleation process significant in the mixture evolution. That is, ΔP_m and the corresponding value of y_m characterize the onset of flashing. Except for the inhomogeneity factor ψ, the parameter a is directly related to the vessel temperature, $\bar{T}_{\mathrm{d}}$. Consequently, in discharge problems the onset of flashing is basically determined by vessel temperatures and substance properties, whereas such a flashing threshold hardly depends on other relevant data as inlet subcooling or nozzle geometry.

Using the stretched variables b and s, defined by the resulting value of ΔP_m and the corresponding values of β, η and y_m, Eq. (32) reduces to

$$b(s) = s \pm \int_{-\infty}^{s} (s-x)^{3/2} \mathrm{e}^{b(x)}\, \mathrm{d}x. \tag{42}$$

Last equation describes the pressure undershoot profile in the nucleation layer and its solution matches at $s \to -\infty$ with the metastable solution (34) at $y = y_m$. The plus and minus signs in Eq. (42) correspond respectively to positive and negative values of the coefficient multiplying the volumetric ratio derivative in Eq. (32) evaluated at point y_m,

$$\frac{\phi^2}{A_m^2} + \frac{\Delta P_m}{\theta_{\mathrm{d}}} - 1 = -2\Delta P_{\mathrm{d}} + \left(2 + \frac{1}{\theta_{\mathrm{d}}}\right)\Delta P_m - 1. \tag{43}$$

In the previous analysis, the smallness of quantities η and $\beta/\Delta P_{\mathrm{m}}$ is an essential hypothesis. To check the validity of that assumption use expression (39), which is equivalent to the equality between $2\beta/\Delta P_m$ and $\Delta P_m^2/a$. This last quantity can be considered very small because the bubble production coefficient, C, takes exponentially high values (see relation (41)). Provided that A'_m is of order unity, (38) implies that β are of the same order than η. Thus β and η are much smaller than ΔP_m, that usually is at most of order unity.

The two possible solutions of Eq. (42), corresponding to both sign possibilities, are drastically different (see Fig. 2). What of them is applicable determines the flow regime downstream from the nucleation layer. Thus, to solve the boundary value problem defined by Eqs. (28) and (32) and conditions (29) and (30), both possible signs of quantity (43) must be considered.

Case 1. Quantity (43) is positive. In such a case, at $s \to \infty$ the nucleation layer solution (plus sign in Eq. (42)) presents exponential growth (see Fig. 2) and matches with a runaway solution of the system (28) and (32). In this runaway solution, volumetric ratio and pressure undershoot grow exponentially in short lengths (see Appendix B) and the cross-sectional area can be considered constant ($A \simeq A_m$). Consequently, expressions relating volumetric ratio with both pressure and pressure undershoot readily follow from Eqs. (26) and (27):

$$P = -\Delta P_m - \frac{\phi^2}{A_m^2} w,$$

$$\Delta P = \Delta P_m + \frac{\phi^2}{A_m^2} w + \theta_{\mathrm{d}} \left[\exp\left(\frac{\phi^2 w^2}{A_m^2 \theta_{\mathrm{d}}^2} - \left(1 - \frac{\Delta P_m}{\theta_{\mathrm{d}}}\right) \frac{w}{\theta_{\mathrm{d}}} \right) - 1 \right].$$

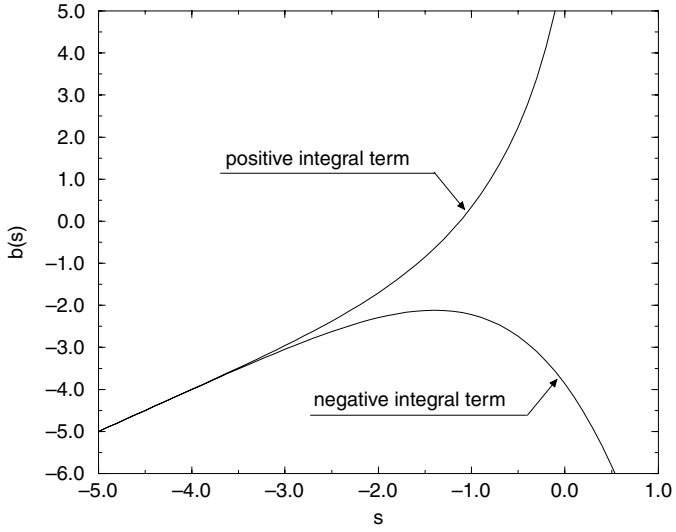

Fig. 2. Solutions of integral equation (42).

To confirm the validity of the asymptotic method previously described, a solution obtained by direct numerical integration of the system (26)–(29) is represented in Fig. 3(a). Pressure and pressure undershoot evolves linearly until a certain pressure undershoot is reached, after which pressure, pressure undershoot and volumetric ratio evolve exponentially in a very short length (Here $\Delta P_m = 0.565\ldots$ and, as a result, quantity (43) is positive).

Therefore, if the exterior pressure is higher or equal than the minimum attainable pressure in the metastable region ($P_a \geqslant -\Delta P_m$), the exit boundary condition (30) can be imposed in Eq. (34) (see also Eq. (36)) to determine the nozzle mass flux

$$\phi^2 = -2\Delta P_d - 2P_a. \tag{44}$$

Otherwise ($P_a < -\Delta P_m$) the ambient pressure will be reached in the runaway solution for the volumetric ratio

$$w_a = -\frac{P_a + \Delta P_m}{\phi^2} A_m^2.$$

As has been aforementioned, the nucleation layer characteristic length, η, is much smaller than unity. Moreover, in Appendix B is proven that the runaway solution attains the volumetric ratio w_a inside a length of order $\eta^{3/5}$. Therefore, provided that quantity (43) is positive and $P_a < -\Delta P_m$, the boundary of the metastable region is approximately at the exit ($y_m \simeq 1$ and $A_m \simeq 1$) and, from a practical point of view, the nozzle mass flux becomes independent of the exterior pressure (see relation (40))

$$\phi^2 \simeq \phi_c^2 = -2\Delta P_d + 2\Delta P_m. \tag{45}$$

Such a practical expression of the *critical* mass flow rate, ϕ_c, corresponds to the boundary condition

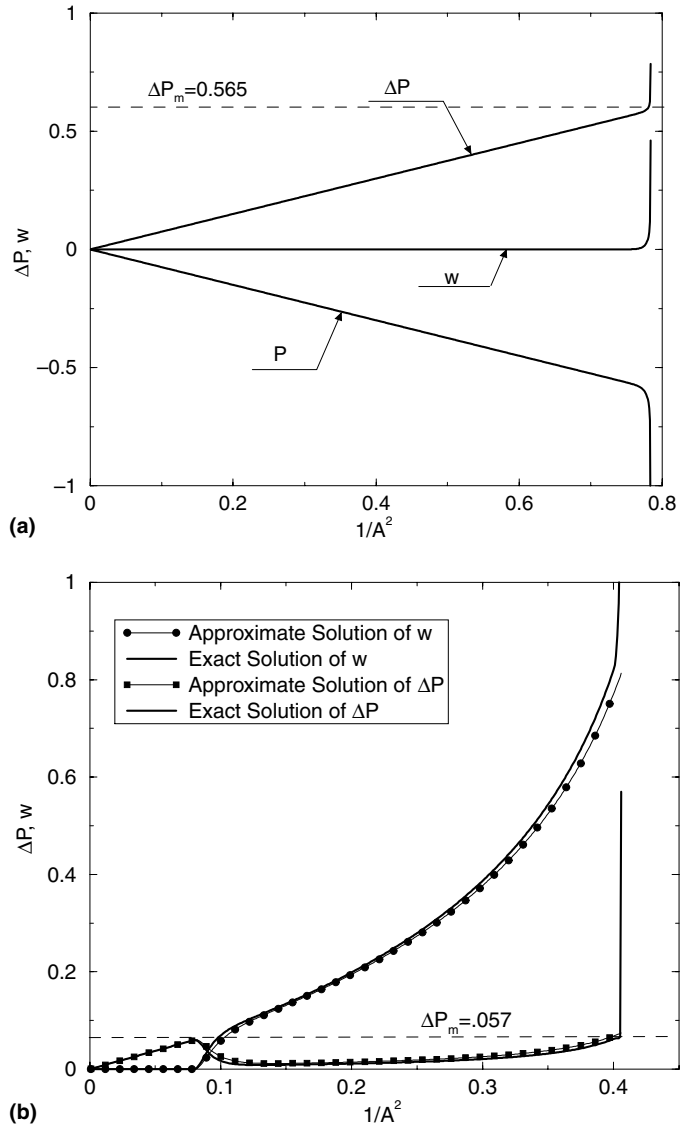

Fig. 3. Numerical solutions of the system (26)–(29) for $\Delta P_{\mathrm{d}} = 0$, $\phi^2 = 1.5$, $\theta_{\mathrm{d}} = 5$, $\log\left(\frac{C\theta_{\mathrm{d}}^3}{\phi^{5/2}\varepsilon^{9/2}\beta^{3/2}}\right) = 70$ and, respectively, $a = 20$ in (a) and $a = 0.2$ in (b).

$$P(1) = -\Delta P_m, \tag{46}$$

which is equivalent to the dimensional expression

$$\bar{P}(z_{\mathrm{a}}) = \bar{P}_{\mathrm{sd}} - \overline{\Delta P}_m.$$

The above condition corrects the HEM critical condition (14), corresponding to high inlet subcoolings, when metastability effects are taken into account.

Case 2. When the onset of flashing, $-\Delta P_m$, and the inlet subcooling, $-\Delta P_d$, are small enough to imply negative values of quantity (43), the nucleation layer is described by Eq. (42) with negative integral term. The corresponding solution passes through a maximum and decreases when s tends to infinity (see Fig. 2).

After such a nucleation layer, the integral member of Eq. (28) can be asymptotically evaluated (see, f.i., Bender and Orszag, 1978 or Murray, 1984) and, as a result, the volumetric ratio can be approximated by

$$w(y) = \begin{cases} 0, & y < y_m, \\ \dfrac{q}{(1+(P(y)/\theta_d))}\left(\displaystyle\int_{y_m}^{y} \frac{A(\bar{y}_0)\log\left(1+(\Delta P(\bar{y}_0)/(\theta_d+P(\bar{y}_0)))\right)}{(1+w(\bar{y}_0))\left(1+(P(\bar{y}_0)/\theta_d)\right)^{1/3}}\,\mathrm{d}\bar{y}_0\right)^{3/2}, & y > y_m. \end{cases} \tag{47}$$

The parameter q depends on the evolution of the pressure undershoot in the nucleation layer, obtained numerically from Eq. (42). To be exact

$$q = \frac{\phi^3 |A'_m|^{3/2}(2a)^{1/2}(1-(\Delta P_m/\theta_d))^{3/2}}{A_m^6 \Delta P_m^{3/2}\left|(\phi^2/A_m^2)+(\Delta P_m/\theta_d)-1\right|\left|\log(1-(\Delta P_m/\theta_d))\right|^{3/2}} \int_{-\infty}^{\infty} \mathrm{e}^{b(x)}\,\mathrm{d}x$$

and

$$\int_{-\infty}^{\infty} \mathrm{e}^{b(x)}\,\mathrm{d}x = \lim_{s\to\infty} \frac{-b(s)}{s^{3/2}} = 1.135\ldots,$$

where b is the solution of Eq. (42) with negative integral term. Physically, the non-dimensional quantity q sizes the number of nuclei which are produced in the nucleation layer and govern the phase interchange downstream.

The differential system

$$\frac{\mathrm{d}w^{2/3}}{\mathrm{d}y} = \frac{-1}{1+(P/\theta_d)-(\phi^2 w/A^2\theta_d)}\left[\frac{2\phi^2 A'(1+w)w^{2/3}}{3A^3} - \frac{q^{2/3}A}{1+w}\log\left(1+\frac{\Delta P}{\theta_d+P}\right)\right], \tag{48}$$

$$\frac{\mathrm{d}\Delta P}{\mathrm{d}y} = \frac{-1}{1+(P/\theta_d)-(\phi^2 w/A^2\theta_d)}\left[\left(1+\frac{P}{\theta_d}\right)\frac{\phi^2 A'(1+w)}{A^3} - \frac{3w^{1/3}}{2}\left(\frac{\phi^2}{A^2} - \left(1+\frac{P}{\theta_d}-\frac{\phi^2 w}{A^2\theta_d}\right)\right.\right.$$
$$\left.\left.\times\left(1+\frac{P+\Delta P}{\theta_d}\right)\right)\frac{q^{2/3}A}{1+w}\log\left(1+\frac{\Delta P}{\theta_d+P}\right)\right], \tag{49}$$

describing the evolution of volumetric ratio and pressure undershoot for $y > y_m$, is obtained from relations (27), (32) and (47). Such a system must be completed with the algebraic Eq. (26) to relate the magnitudes $P, \Delta P$ and w. The solution of (48) and (49) which corresponds to the initial conditions

$$w(y_m) = 0, \quad \Delta P(y_m) = \Delta P_m, \tag{50}$$

matches with the nucleation layer solution at y_m and is valid downstream as long as the pressure undershoot, ΔP, remains small enough.

If ΔP goes beyond the value ΔP_m at any point y_1 downstream from y_m, the system (48) and (49) (or equivalently (47) and (32)) stops being valid and the primitive equations (28) and (32) must be taken into account again. To be exact, the more adequate approximation of Eq. (28)

$$w(y)\left(1+\frac{P(y)}{\theta_d}\right)=q\left(\int_{y_m}^{y}\frac{A(\bar{y}_0)\log\left(1+(\Delta P(\bar{y}_0)/(\theta_d+P(\bar{y}_0)))\right)}{(1+w(\bar{y}_0))\left(1+(P(\bar{y}_0)/\theta_d)\right)^{1/3}}\,d\bar{y}_0\right)^{3/2}$$
$$+\frac{C\theta_d^3}{\phi^{5/2}\varepsilon^{9/2}l^{3/2}}\int_{y'_m}^{y}\left(\int_{y_0}^{y}\frac{A(\bar{y}_0)\log\left(1+(\Delta P(\bar{y}_0)/(\theta_d+P(\bar{y}_0)))\right)d\bar{y}_0}{(1+w(\bar{y}_0))\left(1+(P(\bar{y}_0)/\theta_d)\right)^{1/3}}\right)^{3/2}$$
$$\times\frac{A}{1+w(y_0)}e^{-a/\Delta P(y_0)^2}\,dy_0, \tag{51}$$

should be employed for $y>y_m$ instead of (47) (y'_m can be any value greater than y_m and less than y_1). Eq. (51) reduces to (47) in the interval $y_m\leqslant y\leqslant y_1$ because the last term of (51) is negligible. However, when ΔP approaches ΔP_m at $y=y_1$, the derivative of such an additional term becomes important and the behavior of the first term in the second member of Eq. (32) changes abruptly.

Physically, a secondary nucleation layer arises at section $A_1=A(y_1)$ and, as well as it comes up at section A_m, two possible situations must be considered within the limits of Case 2.

Case 2.1. If the coefficient multiplying the volumetric ratio derivative in Eq. (32) (calculated at point y_1)

$$\left(\frac{\phi^2}{A_1^2}-\left(1+\frac{P_1}{\theta_d}-\frac{\phi^2 w_1}{A_1^2\theta_d}\right)\left(1+\frac{P_1+\Delta P_m}{\theta_d}\right)\right) \tag{52}$$

is positive, the last term of (51) becomes dominant inside of the new nucleation layer. Therefore, just as it happened after y_m when quantity (43) was positive (Case 1 above), both volumetric ratio and pressure undershoot grow exponentially downstream from position y_1 (see Appendix B). Magnitudes evolve in short lengths and the cross-sectional area can be considered approximately constant. As a result, the following relation between pressure and volumetric ratio is obtained from Eq. (27):

$$P+\frac{\phi^2}{A_1^2}w=P_1+\frac{\phi^2}{A_1^2}w_1. \tag{53}$$

Case 2.2. If quantity (52) were negative, after the second nucleation layer the pressure undershoot would decrease and the volumetric ratio would follow the approximate law:

$$w(y) = \frac{q}{(1+(P(y)/\theta_d))}\left(\int_{y_m}^{y} \frac{A(\bar{y}_0)\log\left(1+(\Delta P(\bar{y}_0)/(\theta_d+P(\bar{y}_0)))\right)}{(1+w(\bar{y}_0))\left(1+(P(\bar{y}_0)/\theta_d)\right)^{1/3}}\,d\bar{y}_0\right)^{3/2}$$
$$+\frac{q_1}{(1+(P(y)/\theta_d))}\left(\int_{y_1}^{y} \frac{A(\bar{y}_0)\log\left(1+(\Delta P(\bar{y}_0)/(\theta_d+P(\bar{y}_0)))\right)}{(1+w(\bar{y}_0))\left(1+(P(\bar{y}_0)/\theta_d)\right)^{1/3}}\,d\bar{y}_0\right)^{3/2}. \quad (54)$$

The intensity of the secondary nucleation, q_1, would be determined as the coefficient q, analyzing the pressure undershoot evolution in the last nucleation event. The integrodifferential system (32) and (54) would approximately describe the flow downstream from section y_1, after which an additional nucleation layer could arise when the pressure undershoot ΔP_m were again reached. In such a case, depending on whether the pressure undershoot was increasing after the new nucleation point or not, the solution would either end abruptly as in cases 1 and 2.1 or continue as in cases 2 and 2.2. Thus, the treatment of the problem might be extended indefinitely.

However, the situation described in Case 2.2 only arises under exceptional circumstances which go beyond the limits of this work, f.i., the authors have observed a third nucleation layer at the pipe exit in some flow regimes presenting weak primary nucleation ($q^{2/3}\Delta P_m \sim 1$) upstream from strongly convergent zones of the pipe ($|A'| \gg 1$). So, for the sake of brevity, in the following Case 2.2 will not be taken into account and quantity (52) will be considered positive when the pressure undershoot attains the value ΔP_m downstream from y_m. That assumption means that secondary nucleation layers only can arise at the pipe exit ($y_1 \simeq 1, A_1 \simeq 1$), because pressure and volumetric ratio evolve *explosively* after them. When the exterior pressure, P_a, is less than P_1, the corresponding volumetric ratio (see Eq. (53))

$$w_a = w_1 + \frac{(P_1 - P_a)A_1^2}{\phi^2}$$

is reached in lengths of order $\eta^{3/5} \ll 1$ (see Appendix B).

To illustrate the accuracy of the used asymptotic method, as it was done in Case 1 above, a direct numerical solution of the system (26)–(29) has been obtained. In Fig. 3(b), such a solution is compared with the matched asymptotic solutions of Eqs. (33), (48) and (49). Here the flashing threshold is $\Delta P_m = 0.057\ldots$ (which corresponds to a negative value of (43)) and the corresponding value of q (see Eq. (47)) is 4270. Relative errors, which are of the order of

$$\left(\log\left(\frac{C\theta_d^3}{\phi^{5/2}\varepsilon^{9/2}l^{3/2}}\right)\right)^{-1},$$

are very small.

In the light of the obtained results, the following considerations can be done about the non-dimensional mass flow rate, ϕ, which appears as a parameter in the system (48) and (49):

- There exists a *critical* mass flow rate, ϕ_c, such that the unique solution of the initial-value problem (48) and (50) presents the secondary nucleation layer and the matched runaway solution at the nozzle exit (i.e., $\Delta P(1) = \Delta P_m, y_1 = A_1 = 1$). In the following the value P_c will denote the pressure attained at $y_1 = 1$ in such a critical solution.

- If the ambient pressure P_a is greater than the critical one P_c, the mass flow rate is subcritical ($\phi < \phi_c$) and corresponds to the solution of (48) and (50) fulfilling the exit condition (30).
- When the exterior pressure is under the critical value, ambient conditions are reached in the runaway solution starting at $y_1 \simeq 1$ with $P_1 = P_c$ (see Eq. (53)). Therefore, from a practical point of view, the solution fulfills the critical condition

$$P(1) = P_c \quad (\text{or } \Delta P(1) = \Delta P_m), \tag{55}$$

and the mass flow rate is the critical one, $\phi = \phi_c$.

In the non-equilibrium model developed here, the above condition replaces the HEM critical condition (13), which is equivalent to the non-dimensional expressions

$$\phi^2 = \frac{(1 + (P/\theta_d))^2}{1 + (w/\theta_d)(1 + (P/\theta_d))} = \frac{(1 + (P/\theta_d))^2}{1 - \log(1 + (P/\theta_d))}. \tag{56}$$

To obtain such equilibrium expressions, the approximation hypotheses and the non-dimensional variables defined at the beginning of this section have been taken into account. The second equality follows from the equilibrium condition $\Delta P = 0$ and Eq. (26).

The non-equilibrium condition (55) is applicable when quantity (52) is positive. Then, as ΔP_m is strictly greater than zero, non-equilibrium critical mass fluxes fulfill the inequality

$$\phi_c^2 > \frac{(1 + (P_c/\theta_d))^2}{1 - \log(1 + (P_c/\theta_d))}. \tag{57}$$

As a consequence of that, in Case 2, as it happens in Case 1, the EVUT model leads to critical mass fluxes essentially different from those resulting from HEM approach. However, both models give similar results for intense primary nucleation events ($q^{2/3}\Delta P_m \gg 1$). In general, for the same inlet conditions non-equilibrium critical mass fluxes are greater than equilibrium ones, although such a property cannot be directly inferred from relations (56) and (57). In fact, because of the complexity of problems (48)–(50), demonstrating all the previous assertions rigorously is a very difficult task and exceeds the scope of this work. Alternatively, to illustrate the behavior commented above, Figs. 4–7 are included. Non-equilibrium pressure and pressure undershoot profiles relative to various flow regimes are represented in each figure for typical values of ΔP_m, θ_d and q. Moreover, these curves are compared with the corresponding HEM pressure profiles ($\Delta P = 0$).

The non-equilibrium solutions attain their validity bound $(1/A)_{max}$, which corresponds to the second point where the equality $\Delta P = \Delta P_m$ is fulfilled, at distances greater than those reached by the turning point of the corresponding HEM profile. Therefore, as increasing mass flow rates reduce the validity interval of solutions in both models, non-equilibrium critical solutions ($(1/A)_{max} = 1$) correspond to mass fluxes greater than those given by the homogeneous model. However, when the primary nucleation is very intense ($q^{2/3}\Delta P_m \gg 1$, Figs. 5 and 7), both non-equilibrium and HEM solutions have approximately the same interval of validity and lead to similar critical results.

To sum up, as well as it happened in the homogeneous model, two possible types of critical conditions can arise in the non-equilibrium model developed here. Their applicability depends on whether quantity (43) is positive or not: on the one hand, if (43) is positive (Case 1), critical condition (46) applies; on the other hand, condition (55) corresponds to negative values of (43) (Case 2).

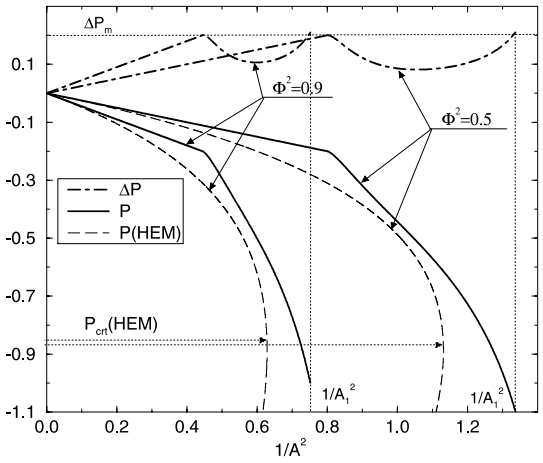

Fig. 4. EVUT pressure and pressure undershoot profiles for $\Delta P_m = 0.2$, $q = 1000$ and $\theta_d = 5$.

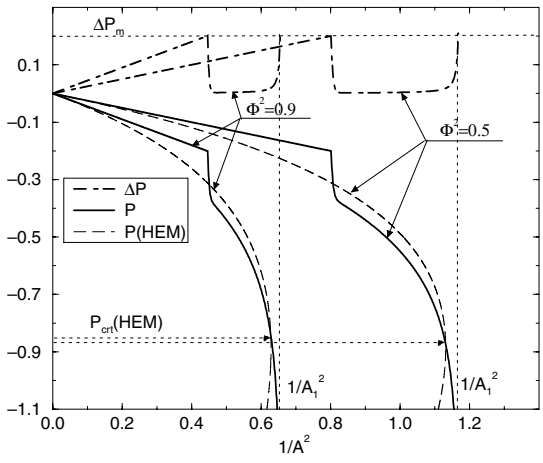

Fig. 5. EVUT pressure and pressure undershoot profiles for $\Delta P_m = 0.2$, $q = 10^5$ and $\theta_d = 5$.

The inequality (15), which determines the range of applicability of the HEM critical conditions, is equivalent to the non-dimensional expression $-2\Delta P_d - 1 \geqslant 0$. Since last inequality represents a weaker condition than the positiveness of quantity (43), the EVUT subcooled critical condition (46) applies in a wider range than the corresponding HEM condition (14). Furthermore, in those cases where the flashing threshold fulfills $\Delta P_m > \theta_d/(1 + 2\theta_d)$, the quantity (43) is always positive and only critical condition (46) is applicable.

In both Cases 1 and 2, the critical condition consists of equating the exit pressure to a critical value ($-\Delta P_m$ in Case 1 and P_c in Case 2), which is uniquely determined by the inlet conditions. If the ambient pressure is greater than such a critical value, the discharge problem is non-critical and leads to subcritical mass fluxes when exit condition (30) is applied. However, when exterior pressures are less than the critical one, apparently the fluid always discharges at critical mass flux ($\phi = \phi_c$). Actually, in these cases the critical pressure is attained shortly before the pipe exit,

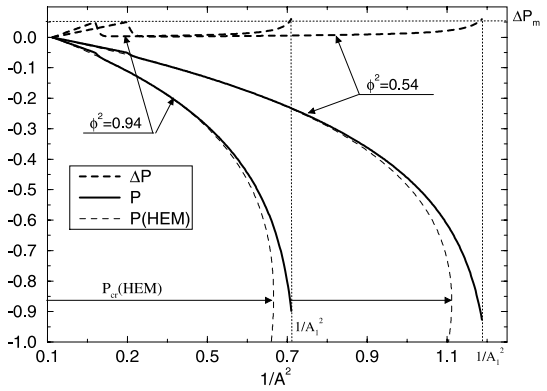

Fig. 6. EVUT pressure and pressure undershoot profiles for $\Delta P_m = 0.05$, $q = 5000$ and $\theta_d = 5$.

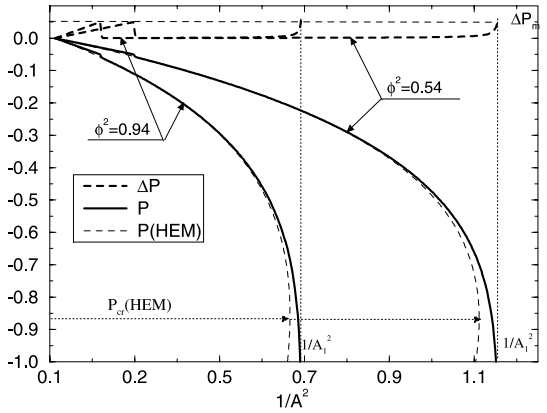

Fig. 7. EVUT pressure and pressure undershoot profiles for $\Delta P_m = 0.05$, $q = 10^5$ and $\theta_d = 5$.

because pressures evolve steeply after reaching the critical value. Therefore, although for subcritical exterior pressures condition (30) is also fulfilled, the discharge mass flow rate is approximately critical.

Subcritical mass fluxes are easily related to exit pressures when such pressures are greater than $-\Delta P_m$ (see (44)). On the other hand, when P_a is between P_c and $-\Delta P_m$ in Case 2, the mass flow rate must be determined by a shooting procedure (in which the solution of the initial-value problem (48)–(50) is forced to fulfill condition (30)).

5. Comparison with experiments

To check the validity of the analytical model developed in Sections 2 and 4, the obtained results are compared with experimental data extracted from the Marviken full-scale tests documentation (The Marviken Project, 1982).

From the Marviken data, three magnitudes are specially significant for this work: vessel pressure, pipe inlet temperature and exit mass flow rate. Rather than measure directly mass flow

rates, in Marviken the mass fluxes were inferred from other experimental data. Basically two techniques were employed: the analysis of the vessel mass evolution and the so-called Pitot–Static technique, consisting of coupling the pressure differences in the pipe-nozzle duct with the measured exit densities. The results corresponding to both methods will be considered here.

According to the analytical models previously developed, in critical discharges the mass flow rate is determined by the stagnation magnitudes existing at the pipe entrance, $\bar{P}_{\mathrm{d}}$ and $\bar{T}_{\mathrm{d}}$. The remaining necessary data are invariable and are extracted from both steam-water thermalhydraulic tables and the geometric data of the experimental device. Only the inhomogeneity factor, ψ is not easily predictable and will be empirically determined.

For the analyzed Marviken tests, where vessel temperatures oscillate between 500 and 530 K and depressurization rates at the exit nozzle are of the order of 10^8 Pa/s, inhomogeneity factors ranging from 10^{-4} to 10^{-3} follow from the empirical formulae given by Elias and Chambré (1993) and Alamgir and Lienhard (1981). However, last authors alert about the applicability of their correlation for depressurization rates below 4×10^8 Pa/s. On the other hand, Elias and Chambre observe that their formula gives rise to large errors in the prediction of pressure undershoots in some specific tests (in particular, they mention the vessel pressure undershoots measured in Marviken experiments). In fact, results are very sensible to ψ variations, for instance, when ψ ranges from 0.0002 to 0.0004, calculated pressure undershoots deviate by 20% below and above the values given by the experimental data of Marviken test 24.

In the present work, the inhomogeneity factor is settled to the fixed value $\psi = 0.00031$, which is determined adjusting the mass flow rates measured at the initial instants of Marviken test 24 to the corresponding experimental values of vessel pressure and temperature. Such a value is of the order of these calculated with the mentioned empirical correlations and, as it will be seen later, in spite of the particular data used in its determination, the agreement between analytical and experimental results will be very acceptable.

Four Marviken experiments have been chosen for the comparative analysis, two saturated blowdowns (Marviken tests 10 and 23) and two subcooled ones (tests 15 and 24). Tests 23 and 24 correspond to discharges through a very short exit nozzle that presents a length to diameter ratio of 0.3, whereas nozzles used in tests 10 and 15 are longer with length to diameter ratios of 3.1 and 3.6, respectively.

To determine the theoretical mass flow rates resulting from these experimental data, the time histories of the non-dimensional inlet subcooling and the non-dimensional flashing threshold (see formula (41)) are evaluated and outlined in Figs. 8 and 9. In the performed calculations, to minimize the errors that could introduce the ideal gas law for the measured working temperatures, the approximate expression (7) is used instead of the second relation of (4). Therefore, the corresponding non-dimensional parameters must be calculated having into account the modified expressions (31).

In all cases the flashing threshold (ΔP_m), which is very insensible to fluctuations of the input parameters, is greater than 0.5 all through the experiment. Then, as quantity (43) is ever positive, only the Case 1 described in Section 4 is applicable and the EVUT critical mass flow rate is always given by expression (45).

In Figs. 10 and 11, both HEM (long dashed line) and non-equilibrium (solid line) analytical mass fluxes are compared with the experimental results obtained in tests 24 and 15. In the first twenty seconds of each test, corresponding to their subcooled stages (see Fig. 9), the EVUT model ap-

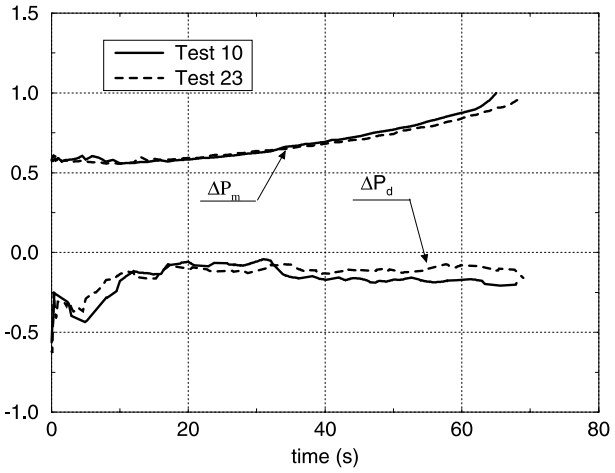

Fig. 8. *Marviken tests 10 and 23:* Vessel subcooling, ΔP_{d}, and flashing threshold, ΔP_m, evolutions.

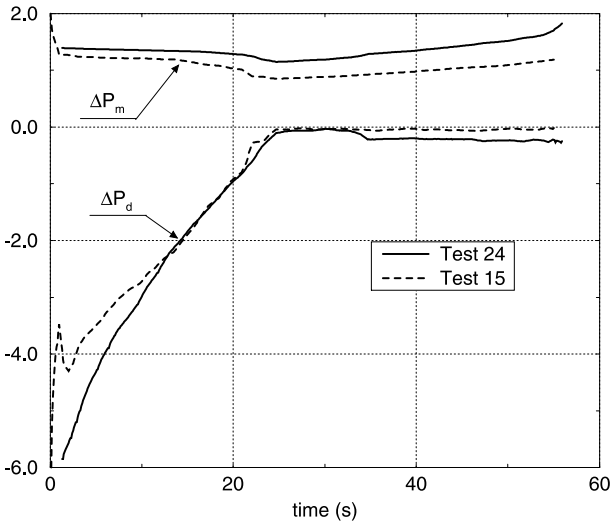

Fig. 9. *Marviken tests 15 and 24:* Vessel subcooling, ΔP_{d}, and flashing threshold, ΔP_m, evolutions.

proximates acceptably the experimental mass flow rates. However, during the saturated stages of these tests the measured mass fluxes, which always take intermediate values between those resulting from both analytical models, are not well predicted by the non-equilibrium formula (45). Moreover, in the latest stage of test 15 the HEM model gives a better approximation to experimental results.

The inability of the non-equilibrium model to evaluate critical mass fluxes properly in saturated blowdowns lies in the fact that in such a model the liquid entering the discharge pipe does not contain vapor nuclei. Such an assumption, which is adequate enough for subcooled inlet conditions ($\Delta P_{\mathrm{d}} < 0$), may be not appropriate in saturated liquids ($\Delta P_{\mathrm{d}} = 0$).

In fact, a lot of bubbles were generated at the beginning of each Marviken experiment, where the abrupt depressurization provokes a high initial supersaturation degree. Some of the bubble

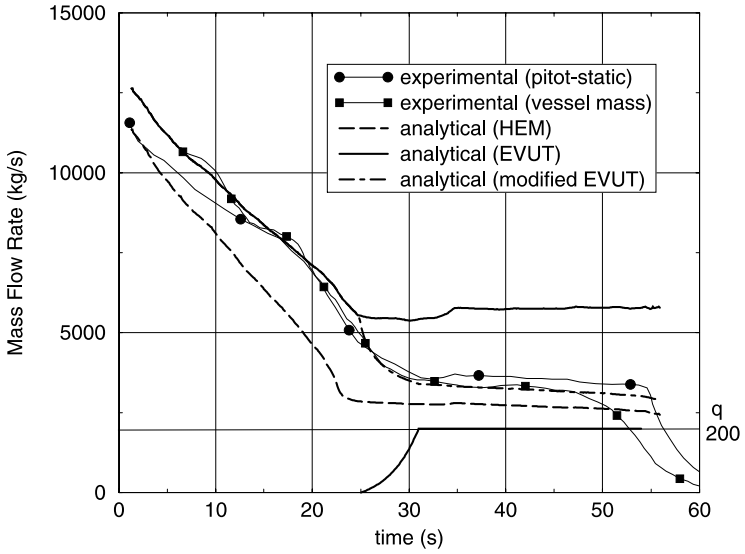

Fig. 10. *Test 24:* Comparison between measured mass flow rates and analytical results (HEM, EVUT and modified EVUT with preexistent bubble nuclei). In last model, the inlet nuclei density, q, is taken so as to adjust experimental and analytical results.

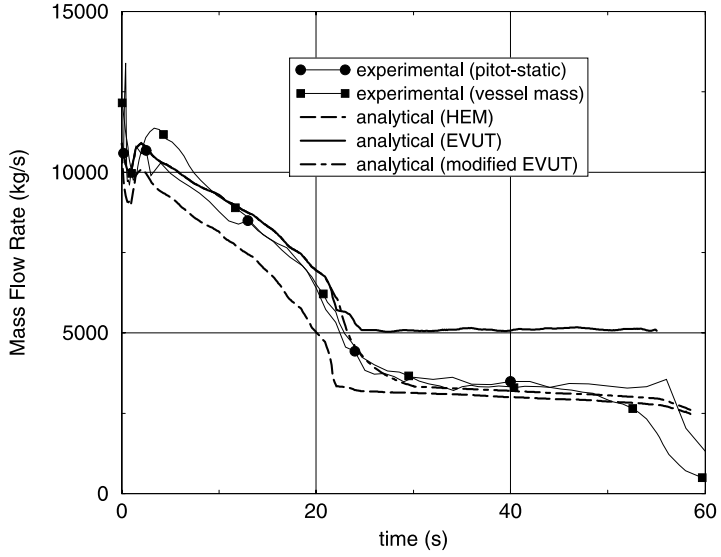

Fig. 11. *Test 15:* Comparison between measured mass flow rates and analytical results (HEM, EVUT and modified EVUT with the inlet nuclei density, q, obtained in test 24).

nuclei produced during that supersaturated stage remained immersed in the surrounding liquid up to they were dragged into the discharge pipe (this phenomenon has been also experimentally observed, see, f.i., the mention done in Deligiannis and Cleaver, 1996).

As a consequence of this, for saturated inlet conditions the fluid no longer must be considered as pure liquid inside of the pipe. Actually, the volumetric ratio evolves along the pipe-nozzle duct following the growth law (51) particularized for $y_m = y'_m = 0$, as if a primary nucleation event arises at the pipe inlet. The parameter q appearing in that expression accounts for the number of nuclei created in the vessel and entering the discharge pipe. In fact, providing that N_d is the bubble number density at the vessel, the following term:

$$\frac{4\pi N_\mathrm{d}\bar{\rho}(z)}{3\bar{\rho}_\ell\bar{\rho}_\mathrm{G}(z)}\left(\int_0^z \frac{2k_\ell\overline{\Delta T}(\bar{z}_0)}{L\bar{\rho}_\mathrm{G}(\bar{z}_0)^{1/3}\bar{v}(\bar{z}_0)}\,\mathrm{d}\bar{z}_0\right)^{3/2}$$

must be added to the second member of the vapor generation law (10). To see that, use the steady version of the conservation equation of bubble number density (see, f.i., Deligiannis and Cleaver, 1990) and the bubble growth law (A.1). Then, after non-dimensionalizing the resulting vapor generation law, the formula (51) with $y_m = y'_m = 0$ and

$$q = \frac{4\pi N_\mathrm{d}}{3}\left(\frac{2k_\ell\bar{T}_\mathrm{d}z_\mathrm{a}}{\phi\bar{P}_\mathrm{sd}\bar{v}_\mathrm{cd}}\right)^{3/2}\left(\frac{\theta_\mathrm{d}}{\varepsilon l}\right)^3, \tag{58}$$

is obtained. Therefore, as long as the second term of the modified equation (51) is negligible, rather than expressions (34) and (36) the more adequate system (48) and (49) must be employed to describe the pipe-nozzle flow.

Then, for saturated inlet conditions, despite the positiveness of quantity (43), rather than formula (45) the procedure described in Case 2 of Section 4 must be used to determine the critical mass flow rate. To be exact, as long as the rare possibility of secondary nucleation events inside of the pipe-nozzle duct is discarded, the critical condition appears as a secondary flashing point arising at the nozzle exit (see condition (55)). The flashing threshold, ΔP_m, would be determined when the derivative of the second term of the volumetric ratio law (51) became significant in relation (32). However, provided that flashing threshold mainly depends on the non-dimensional parameter a, it can be well approximated by the minimal solution of the algebraic relation (41) particularized for $\Delta P_\mathrm{d} = 0$ and a representative value of $|A_m/A'_m|$.

Analytically, the critical mass flow rate, ϕ_c, is determined forcing to the differential system (48) and (49) to have a solution which fulfills the boundary conditions

$$w(0) = \Delta P(0) = 0, \quad \Delta P(1) = \Delta P_m.$$

Making use of that procedure, the dependence of the critical mass flow rate on the vessel nucleation intensity has been evaluated and outlined in Fig. 12 for the inlet conditions measured during the saturated stages of tests 15 and 24.

The critical mass flux decreases from the non-equilibrium value $\sqrt{2\Delta P_\mathrm{m}}$ (see Eq. (45) in Case 1) for $q = 0$ to the HEM result (see Eq. (56)) for $q \to \infty$. However, the equilibrium critical flow is approached in test 15 for vessel nucleation intensities lower than those needed in test 24. Physically, these facts can be explained as follows: first, the greater is the quantity of bubble nuclei entering the discharge pipe (q) the faster is the evolution to equilibrium conditions inside of the pipe-nozzle duct; second, this evolution mainly arises at the exit zone of the nozzle, where the

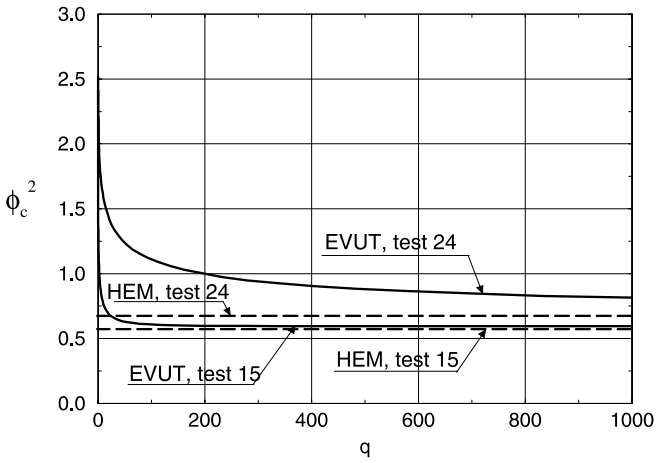

Fig. 12. *Modified EVUT model:* Non-dimensional mass flow rate, ϕ_c, versus nuclei density at the nozzle inlet, q.

pressure undershoot is large enough to make the q-terms significant in Eqs. (48) and (49) (test 15 nozzle possesses a longer exit zone than the one made use of in test 24).

The behavior commented above agrees with the phenomena observed in the saturated stages of tests 24 and 15 (see Figs. 10 and 11). On the one hand, measured mass flow rates behave between the non-equilibrium and equilibrium analytical results. On the other hand, test 15 experimental mass fluxes are closer to HEM values than those measured in test 24.

Determining analytically the value of q applicable to each case would require a precise study of the evolution of some vessel magnitudes. Thus, in order not to prolong excessively this work, in the saturated blowdowns analyzed here the vessel nucleation intensity has been estimated adjusting calculated and measured mass flow rates. The results corresponding to the saturated stages of tests 24 and 23 are outlined in Figs. 10 and 13 (dot–dashed lines), where the values of parameter q used in the calculations are also represented. The value of $q = 200$, obtained during the most part of the saturated blowdowns in both tests, corresponds to inlet bubble number densities (see Eq. (58)) between 0.4×10^{11} and 0.6×10^{11} $1/m^3$. These results are very near to the fixed nuclei density of $N_d = 10^{11}$ $1/m^3$ taken in the two-phase critical flow model of Dobran (1987) to simulate critical discharges of pressurized water. Similarly, in their model Dagan et al. (1993) make use of a fixed inlet nuclei density which depends on the length to diameter ratio of the discharge channel. These authors proposed a value of $N_d = 0.3 \times 10^{11}$ $1/m^3$ for length to diameter ratios equal to unity (a suitable value for the short Marviken discharge nozzles when the effect of the large diameter discharge pipe is neglected).

During the saturated stages of tests 10 and 15 the parameter q is not easily adjustable, because the measured mass fluxes oscillates within the flat zone close to HEM values of the curves outlined in Fig. 12. However, tests 10 and 23, as well as tests 15 and 24, present very similar evolutions of vessel magnitudes, thus the values of parameter q used to approach the experimental data of tests 23 and 24 can be employed to reproduce tests 10 and 15, respectively. In Figs. 14 and 11, the modified EVUT results (dot–dashed lines) are represented, respectively, for test 10 and the saturated stage of test 15. Analytical and experimental data present now an excellent agreement at all times.

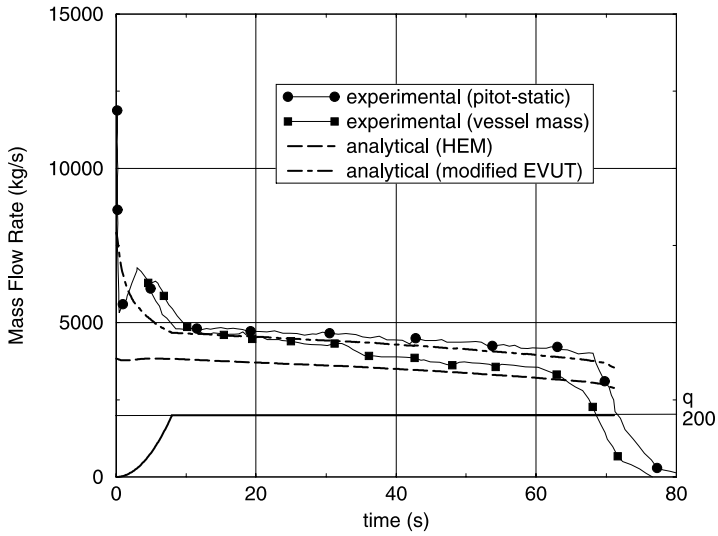

Fig. 13. *Test 23:* Comparison between measured mass flow rates and analytical results (HEM and modified EVUT). In last model, the inlet nuclei density, q, is taken so as to adjust experimental and analytical results.

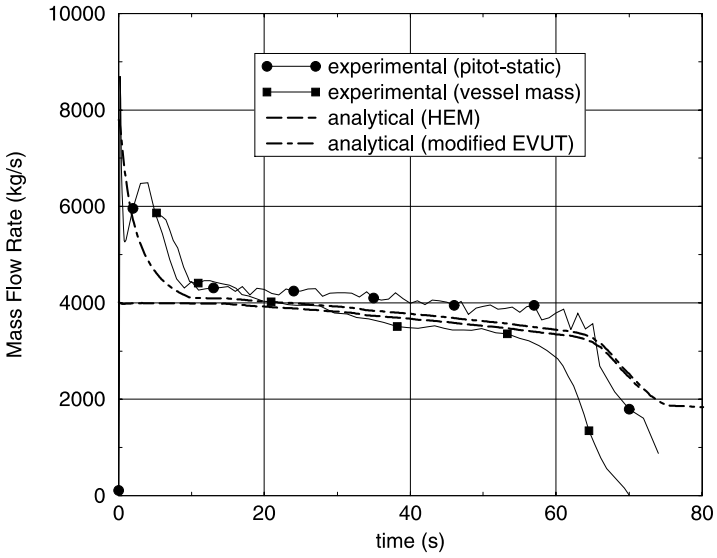

Fig. 14. *Test 10:* Comparison between measured mass flow rates and analytical results (HEM and modified EVUT with the inlet nuclei density, q, obtained in test 23).

To sum up, for the analyzed tests the expression (45) (Case 1) gives a good approximation of critical mass fluxes in subcooled blowdowns. Moreover, when the EVUT model is modified to account for the bubble nuclei present at the pipe inlet, the critical condition (55) (Case 2) also determines very well critical discharges in saturated blowdowns. However, in such cases the parameter q, which account for vessel nucleation intensities, must be previously determined. Finally,

the non-equilibrium model justifies reasonably the validity of HEM model to predict saturated blowdowns through long-sized nozzles as well as its inability to approximate experimental results for subcooled blowdowns or discharges through very short nozzles.

6. Conclusions

An EVUT model has been analyzed to account for thermal disequilibrium in flashing critical flows. The obtained results have been related with those coming from the HEM, whose main features are summed up in Section 3.

In both models, two types of critical flow regimes, basically characterized by the position of the onset of flashing (the point where the vapor phase appears), can arise depending on the inlet subcooling degree. On the one hand, for small or null inlet subcoolings the flashing point is usually attained before the nozzle end. On the other hand, when the subcooling degree at the nozzle intake is high enough, the vapor phase does not appear up to the exit section.

In the HEM approach the onset of flashing coincides with the limit of the saturation zone ($\Delta P = 0$) and the critical boundary conditions corresponding to small and high inlet subcoolings are, respectively, (13) and (14).

In the EVUT model, as well as it happens in the equilibrium model, the vapor phase also appears when the saturation line ($w = 0, \Delta P = 0$) is reached. However, its influence remains negligible up to the pressure undershoot attains a certain flashing threshold ($\Delta P_m > 0$). Then, from a practical point of view the onset of flashing is characterized by conditions $w \simeq 0$ and $\Delta P = \Delta P_m$. The set of applicable critical conditions in this case are (46) and (55), which correspond respectively to positive and negative values of quantity (43). On the one hand, condition (46) means that the unique nucleation layer arises just at the exit section. On the other hand, condition (55) implies that the flashing threshold is attained at the nozzle end for the second time.

The adequacy of the EVUT model to predict critical mass fluxes in subcooled blowdowns is verified after comparing EVUT results to some experimental data obtained in the Marviken test series. However, the non-equilibrium model developed in Sections 2 and 4 considers that only pure liquid without bubbles flows into the nozzle, which results to be an unrealistic hypothesis in saturated blowdowns ($\Delta P_d = 0$). After modifying the EVUT model to take into account the presence of bubble nuclei in the liquid expelled from the vessel, the analytical results are also largely improved for saturated blowdowns. However, the bubble number density entering the discharge nozzle must be adjusted. For the saturated blowdowns analyzed here, the vessel nuclei density needed to fit analytical and experimental results are of the same order than those used in other studies.

Acknowledgements

The authors thank Prof. A. Liñán of the Polytechnical University of Madrid for his suggestions and useful ideas given at the beginning of this work. This work has been partially supported by the Spanish Nuclear Security Commission within the CAMP–Spain program.

Appendix A

Using Eulerian coordinates the bubble growth law (9) takes the form

$$\frac{\mathrm{D}}{\mathrm{D}t}\left(\frac{4\pi}{3}\bar{r}^3\bar{\rho}_{\mathrm{G}}\right)=4\pi\bar{r}\frac{k_\ell\overline{\Delta T}}{L},$$

where the substantial derivative $\mathrm{D}/\mathrm{D}t=\partial/\partial t+\bar{v}\,\partial/\partial z$ is introduced and the value $Nu=2$ is taken. For steady flows such an equation reduces to

$$\frac{\mathrm{d}}{\mathrm{d}z}\left(\frac{4\pi}{3}\bar{r}^3\bar{\rho}_{\mathrm{G}}\right)=4\pi\bar{r}\frac{k_\ell\overline{\Delta T}}{L\bar{v}}$$

which integrated for a bubble sprouting at $z=z_0$ ($\bar{r}(z_0)=0$) gives

$$\bar{r}(z;z_0)=\frac{1}{\bar{\rho}_{\mathrm{G}}(z)^{1/3}}\left(\int_{z_0}^{z}\frac{2k_\ell\overline{\Delta T}(\bar{z}_0)}{L\bar{\rho}_{\mathrm{G}}(\bar{z}_0)^{1/3}\bar{v}(\bar{z}_0)^{1/3}}\,\mathrm{d}\bar{z}_0\right)^{1/2}. \tag{A.1}$$

The bubble production law (8) remains null up to section z_n, where the pressure undershoot becomes non-negative. Therefore, under steady conditions the void fraction *flux* at any section after z_n is determined by the bubbles generated from z_n up to z:

$$\alpha\bar{v}\bar{A}=\int_{z_n}^{z}\frac{4}{3}\pi\bar{r}(z;z_0)^3NB\exp\left(-\frac{16\pi\sigma^3\psi}{3k_{\mathrm{B}}\bar{T}(z_0)\overline{\Delta P}(z_0)^2}\right)(1-\alpha(z_0))\bar{A}(z_0)\,\mathrm{d}z_0.$$

From this relation and Eq. (A.1), the vapor generation law (10) for steady flows readily follows.

Appendix B

The following results hold for blowdowns through frictionless convergent nozzles ($A'<0$):

- First, as long as ΔP remains positive after point y_n (the limit of the subcooled region, $P(y_n)=0$), w is an increasing function of y whereas P and $P+\Delta P$ are decreasing. Moreover, the quantity

$$1+\frac{P}{\theta_{\mathrm{d}}}-\frac{\phi^2 w}{A^2\theta_{\mathrm{d}}} \tag{B.1}$$

is non-negative throughout the nozzle.

- Second, let y_t be a point where the coefficient of the volumetric ratio derivative in Eq. (32) becomes positive. Then, providing that ΔP is positive in the interval $]y_n,y_t]$, the pressure undershoot not only remains positive after $y>y_t$ but it is also increasing.

To prove the first assertion, observe that for $y>y_n$ the positiveness of ΔP imply that the product $w(1+P/\theta_{\mathrm{d}})$ is increasing (derive in Eq. (28)) and, as a result, $P+\Delta P$ is decreasing (use relation (26)). Then, as the y-derivative of $w(1+P/\theta_{\mathrm{d}})$ is positive and the second member of Eq. (27) is negative, the following inequalities are obtained:

$$\left(1+\frac{P}{\theta_{\mathrm{d}}}-\frac{\phi^2 w}{A^2\theta_{\mathrm{d}}}\right)\frac{\mathrm{d}w}{\mathrm{d}y}>0,\quad \left(1+\frac{P}{\theta_{\mathrm{d}}}-\frac{\phi^2 w}{A^2\theta_{\mathrm{d}}}\right)\frac{\mathrm{d}P}{\mathrm{d}y}<0.$$

These strict inequalities prove: firstly, that quantity (B.1), which equals unity at y_n, never is null and remains positive for $y > y_n$; secondly, that w and P are, respectively, increasing and decreasing functions of y.

The second result is now an immediate consequence of the first one, which implies that the coefficient of the volumetric ratio derivative in Eq. (32) goes on being positive for $y > y_t$.

Taking into account the preceding results, the inequality

$$w-w(y_t)=\Delta w \geqslant \frac{2C\theta_{\mathrm{d}}^3(\log(1+(\Delta P_m/(\theta_{\mathrm{d}}-\Delta P_m))))^{3/2}\mathrm{e}^{-a/\Delta P_{\mathrm{m}}^2}}{5\phi^{5/2}\varepsilon^{9/2}l^{3/2}(1-(\Delta P_{\mathrm{m}}/\theta_{\mathrm{d}}))^{3/2}(1+w)^{5/2}}(y-y_t)^{5/2}$$

comes from Eq. (28) for $y > y_t$. Thus, after using the second relation of (38), the following bound is obtained:

$$(y-y_t)^{5/2}\leqslant \frac{5\Delta w(1+w)^{5/2}A_{\mathrm{m}}^{11/2}\left|(\phi^2/A_m^2)+(\Delta P_m/\theta_{\mathrm{d}})-1\right|}{2\phi^2|A_m'|}\eta^{3/2}. \tag{B.2}$$

Expression (B.2) implies that, after any point y_t fulfilling the hypotheses of the second result, magnitude variations of order unity are performed in regions of approximate size $\eta^{3/5}$ (η is the width of the nucleation layer at y_m). In other words, after such points the solutions of the system (28) and (32) behave explosively, reaching large values of volumetric ratio and pressure undershoot in short distances.

The points y_m and y_1 defined in Section 4 fulfill the conditions of the second result for Cases 1 and 2.1, respectively. In particular, in Case 2.1 the second member of Eq. (49) is positive for $\Delta P = 0$. Thus, in the phase plane of the system (48) and (49) the trajectories cannot cross from above the line $\Delta P = 0$ and the pressure undershoot, ΔP, remains positive between points y_m and y_1.

References

Alamgir, M., Lienhard, J.H., 1981. Correlation of pressure undershoot during hot-water depressurization. J. Heat Transfer 103, 52–55.

Ardron, K.H., 1978. A two-fluid model for critical vapour–liquid flow. Int. J. Multiphase Flow 4, 323–337.

Barták, J., 1990. A study of the rapid depressurization of hot water and the dynamics of vapour bubble generation in superheated water. Int. J. Multiphase Flow 16, 789–798.

Bender, C.M., Orszag, S.A., 1978. Advanced Mathematical Methods for Scientists and Engineers. McGraw-Hill, New York.

Bilicki, Z., Kestin, J., 1990. Physical aspects of the relaxation model in two-phase flow. Proc. R. Soc. London A (428), 379–397.

Blander, M., Katz, J.L., 1975. Bubble nucleation in liquids. AIChE J. 21 (5), 833–848.

Bouré, J.A., 1978. In: Two-Phase Flows and Heat Transfer with Application to Nuclear Reactor Design Problems. McGraw-Hill, New York, pp. 157–178 (Chapter 9).

Collins, R.L., 1978. Choked expansion of subcooled water and the IHE flow model. J. Heat Transfer 100, 275–280.

Dagan, R., Elias, E., Wacholder, E., Olek, S., 1993. A two-fluid model for critical flashing flows in pipes. Int. J. Multiphase Flow 19, 15–25.

Deligiannis, P., Cleaver, J.W., 1990. The role of nucleation in the initial phases of a rapid depressurization of a subcooled liquid. Int. J. Multiphase Flow 16, 975–984.
Deligiannis, P., Cleaver, J.W., 1992. Determination of the heterogeneous nucleation factor during a transient liquid expansion. Int. J. Multiphase Flow 18, 273–278.
Deligiannis, P., Cleaver, J.W., 1993. Influence of surrounding bubbles on the rate of nucleation. Int. J. Heat Mass Transfer 36, 3697–3701.
Deligiannis, P., Cleaver, J.W., 1996. Blowdown from a vented partially full vessel. Int. J. Multiphase Flow 22, 55–68.
Dobran, F., 1987. Nonequilibrium modelling of two-phase critical flows in tubes. J. Heat Transfer 109, 731–739.
Elias, E., Chambré, P.L., 1984. A mechanistic non-equilibrium model for two-phase critical flow. Int. J. Multiphase Flow 10 (1), 21–40.
Elias, E., Chambré, P.L., 1993. Flashing inception in water during rapid decompression. J. Heat Transfer 115, 231–238.
Elias, E., Lellouche, G.S., 1994. Two-phase critical flow. Int. J. Multiphase Flow 20, 91–168.
Murray, J.D., 1984. Asymptotic Analysis. Springer, New York.
Nigmatulin, R.I., 1991. Dynamics of Multiphase Media. Hemisphere, New York.
Saha, P., 1978. A review of two-phase steam-water critical flow models with emphasis on thermal nonequilibrium. BLN-NUREG-50907, Brookhaven National Laboratory.
Sami, S.M., Doung, T., 1989. A transient model for predicting nonhomogeneous nonequilibrium critical two-phase flows. Nucl. Technol. 85, 98–108.
The Marviken Project, 1982. The Marviken Full Scale Critical Flow Tests. EPRI-NP–2370, Electric Power Research Institute.
Wallis, G.B., 1980. Critical two-phase flow. Int. J. Multiphase Flow 6, 97–112.